High-performance CO_2-selective Hybrid Membranes by Exploiting MOF-breathing Effects

Aylin Kertik,[§] Lik H. Wee,[§†*] Kadir Sentosun,[‡] Jorge A. R. Navarro,[±] Sara Bals,[‡] Johan A. Martens,[§] Ivo F. J. Vankelecom[§*]

[§]Center for Surface Chemistry and Catalysis, University of Leuven, Celestijnenlaan 200F, Post Box- 2461, B3001, Leuven, Belgium.

[‡]Electron Microscopy for Materials Science, University of Antwerp, Groenenborgerlaan 171, B2020, Antwerp, Belgium.

[±]Departamento de Química Inorgánica, Universidad de Granada, Av. Fuentenueva S/N, 18071 Granada, Spain.

KEYWORDS: metal-organic framework; breathing; crosslinking; mixed-matrix membranes; gas separation

ABSTRACT

Conventional CO_2 separation in the petrochemical industry via cryogenic distillation or amine-based absorber-stripper units is energy intensive and environmentally unfriendly. Membrane-based gas separation technology, on the other hand, has contributed significantly to the development of energy-efficient systems for e.g. natural gas purification. The implementation of commercial polymeric membranes in gas separation processes is restricted by their permeability-selectivity trade-off and by their insufficient thermal and chemical stability. Herein, we present the fabrication of Matrimid®-based membrane loaded with a breathing metal-organic framework

(MOF) (NH_2-MIL-53(Al)) which is capable of separating binary CO_2/CH_4 gas mixtures with high selectivities without sacrificing much of its CO_2 permeabilities. NH_2-MIL-53(Al) crystals were embedded in a polyimide (PI) matrix and the mixed–matrix membranes (MMMs) were treated at elevated temperatures (up to 350 °C) in air to trigger PI crosslinking and to create PI-MOF bonds at the interface to effectively seal the grain boundary. Most importantly, the MOF transitions from its narrow-pore form to the large-pore form during this treatment, allows the PI chains to partly penetrate the pores and crosslink with the amino functions at the pore mouth of the NH_2-MIL-53(Al) and stabilizes the open-pore form of NH_2-MIL-53(Al). This crosslinked MMM, with MOF pore entrances made more selective by the anchored PI-chains, achieves outstanding CO_2/CH_4 selectivities. This approach provides significant advancement towards the design of selective MMMs with enhanced thermal and chemical stabilities which could also be applicable for other potential applications, such as separation of hydrocarbons (olefin/paraffin or isomers), pervaporation and solvent resistant nanofiltration.

Introduction

Purification of natural gas, also known as natural gas sweetening, is the largest industrial separation involving removal of CO_2 from CH_4.[1-3] Many natural gas wells contain significant amounts of CO_2, which have to be removed prior to delivery to pipelines to minimise corrosion and to increase calorific value.[1] Raw biogas generated from biomass and organic wastes contains primarily of 55-65% of methane and 35-45% of CO_2. Biogas upgrading to achieve biomethane with concentration above 90% similar to the natural gas standard is of economic importance. Both types of gas upgrading can very well be performed with membrane technology.

Among the membranes developed for gas treatment, only polymeric membranes have been commercialized so far.[6,7] An important search is still ongoing for membranes with higher selectivity without permeance loss, together with enhanced thermal and chemical stability.[7] Currently, the typical CO_2/CH_4 selectivity in industrial separations is limited due to the permeability-selectivity trade-off for polymeric membranes, as reflected in the Robeson upper-bound.[1,8,9] Another major challenge of polymer membranes for gas separation is related to their susceptibility to plasticization at high CO_2 partial pressures when polymer membranes encounter an undesirable loss in separation power. CO_2 then excessively swells the polymer and eases the permeation of CH_4, thus reducing selectivities.[6] Membrane crosslinking is one of the best ways to handle this plasticization.[10-12]

Mixed-matrix membranes (MMMs) composing of homogeneously dispersed fillers in a polymeric matrix aim to combine the advantageous of polymer processibility and the superior separation properties of the porous fillers.[13-19] Metal-organic frameworks (MOFs) have attracted considerable attention owing to their tailorable functionality, tunable pore size and breathing effects.[20,21] Breathing of MOFs refers to a structural transition, involving the reversible opening or contraction of pores.[22,23] MIL-53 is one of the best representatives of such "breathing" MOFs.[24] It is constructed from $MO_4(OH)_2$ octahedra (M= Fe^{3+}, Cr^{3+}, Al^{3+} or Ga^{3+}) and terephthalate (BDC) linkers, exhibiting the unique transition of large-pore (*lp*, 8.5 Å x 8.5 Å) to narrow-pore (*np*, 2.6 Å x 13.6 Å) form by inducing a unit cell volume change upon the inclusion of guest molecules (e.g. water, CO_2 and xylene) or external stimuli (e.g. pressure and heat).[24-28] As-synthesized MIL-53 consists of trapped unreacted BDC molecules in the pores and gives the *lp* configuration. These BDC species can be evacuated upon heating at 320 °C, resulting in an open-pore framework. The open-pore framework will absorb water molecules upon cooling to room temperature to give the

np configuration. The absorbed water molecules interact with the hydroxyl groups of the inorganic cluster through strong H-bonding. The breathing MIL-53(Al) is known for its unusually high adsorptive selectivity for CO_2 over CH_4 via the quadrupolar interaction of CO_2 with the corner-sharing hydroxyl groups of the MIL-53 pore wall.[29] A similar topology but with amine-functionalization could be synthesized by replacing the terephthalic acid with 2-aminoterephthalic acid.[30-32] NH_2-MIL-53(Al) has diamond shaped channels with a pore diameter of 7.5 x 7.5 Å and with amino groups that point inwards to the pore.[32] Unlike many amino-functionalized materials, NH_2-MIL-53(Al) does not form a chemical bond between CO_2 molecules and the NH_2 groups. Instead, the amino functions regulate the breathing behaviour, resulting in superior separation factor for CO_2 over CH_4.[25] The interaction of the decorated amino functions with the aluminium-occupied oxygen octahedra in the framework structure stabilizes the NH_2-MIL-53(Al) *np* form via hydrogen bonding. As a result, the energy losses associated with the structural perturbations upon formation of the *np* structure is reduced, and thus contributing towards the enhanced local flexibility of the inorganic trans-corner-sharing [AlO_6] chains. This synergistic effect leads to NH_2-MIL-53(Al) structure with greater structural stability in its *np* form. The stable *np* starting form allows it to effectively pack CO_2 molecules while exclusively hindering the adsorption of other molecules with larger kinetic diameter such as CH_4. Moreover, the presence of structural amino and hydroxyl functional groups in MIL-53 also play an important role to enhance the host-guest interaction with CO_2, contributing to a high CO_2/CH_4 selectivity.[25]

Excellent selectivities have been recently reported using CuBDC nanosheets[33] or ZIF-8[34] as MOF fillers in MMMs for CO_2/CH_4 separations. NH_2-MIL-53 as a powder possessed high selectivity in CO_2/CH_4 separation, but failed to reach the 2008 Robeson upper bound for CO_2/CH_4 in MMM separations, especially due to low selectivities. Probably, this is mainly due to polymer-

MOF interstitial defects and the too open pore configuration of the MOF in the membranes. The results highlight the challenge to regulate the MOF breathing behaviour to enable their use in selective membrane gas separations.[35,36] Recently, we reported an in-situ thermally induced amorphization of ZIF-8 in a PI matrix. The thermal treatment simultaneously enhances MOF-PI interactions via oxidative crosslinking to effectively seal the interfacial voids/grain boundaries. This new hybrid crosslinked membrane showed enhanced chemical and thermal stabilities, together with very high CO_2/CH_4 mixed gas selectivities.[37] In present work, the remarkable breathing effect of NH_2-MIL-53(Al) MOF is exploited by maintaining the *lp* structure, regardless guest molecule, pressure or temperature, via controlled thermal treatment of the MOF at 350 °C while embedded in the polymer matrix. During this treatment, the PI membrane matrix is crosslinked. Simultaneously, the polymer chains are penetrated into the *lp* pores, where they link covalently to the amino functions decorated on the pore walls of NH_2-MIL-53(Al). Upon cooling, the MOF retains the *lp* form, while the region around the pore mouth gets densified and became more selective. The *lp* structure of NH_2-MIL-53(Al) anchored with polymer chains at the pore mouth shows remarkable selectivity in CO_2/CH_4 separation, while retaining the membrane permeabilities.

Experimental Methods

Materials

Commercially available polyimide (PI, Matrimid 5218) was kindly provided by Huntsman and used after drying at 110 °C overnight. For NH_2-MIL-53(Al) synthesis, the linker source 2-aminoterephthalic acid (NH_2BDC, $H_2NC_6H_3$-1,4-$(CO_2H)_2$, 99+%) and the Al source aluminum nitrate nonahydrate ($Al(NO_3)_3.9H_2O$, 98.5+%) were obtained from ChemLab and Acros Organics,

respectively, and used without further treatment. The solvents used in the solvent exchange and membrane preparation were dimethylformamide (99+%), chloroform (99.8%), and methanol (99.8%), purchased from Acros Organics.

Synthesis of NH_2-MIL-53(Al)

The synthesis of NH_2-MIL-53(Al) was achieved by dissolving NH_2BDC (2 g) and $Al(NO_3)_3.9H_20$ (2 g) in distilled water (400 mL). The solution was stirred at 100 °C for 6 hours. Upon cooling, the MOF particles were separated by centrifugation and washed using DMF, methanol and chloroform, respectively. Following the final centrifugation step, the remaining MOF sludge was re-distributed in $CHCl_3$ and stored in wet form. The synthesis of NH_2-MIL-53(Al) nanoparticles was carried out by dissolving $Al(NO_3)_3 \cdot 9H_2O$ (0.7602 g) in 7.50 ml of distilled water and NH_2BDC (0.5601 g) in 22.50 ml of DMF.[49] After mixing the two solutions and stirring for 1 h, the final solution was transferred into a 100 ml stainless steel autoclave, followed by inducing reaction at 150 °C for 24 h. Upon cooling, the synthesized MOF particles were separated by centrifugation and washed with DMF, methanol and chloroform, respectively. After the final centrifugation step, the collected MOF sludge was re-distributed in $CHCl_3$ and stored in wet form.

Fabrication of PI-NH_2-MIL-53(Al) MMMs

MMMs with 20, 30 and 40 wt% MOF loadings were fabricated. MOF mixture was weighed to provide the MOF content to achieve the desired MOF loading and the Matrimid® that was dried overnight at 110 °C was added and dissolved to this mixture. A polymer concentration of 7 wt% was kept to achieve a moderately viscous solution that still allows membrane casting, but would prevent MOF precipitation upon casting. The membrane mixture was stirred until the polymer was fully dissolved. Proving the effectiveness of membrane preparation starting from a MOF sludge,

extra mixing step with e.g. ultrasonication was not needed in order to achieve excellent MOF particle distribution. The MOF loading of membranes was calculated as given in the following equation:

$$\text{Loading (wt.\%)} = 100 * \frac{\text{wt}_{\text{MOF}}}{\text{wt}_{\text{MOF}} + \text{wt}_{\text{polymer}}}$$

where, wt_{MOF} and $\text{wt}_{\text{polymer}}$ are amount of MOF and polymer, respectively. Petri dishes specifically designed for membrane casting were used to ensure uniform membrane thickness. The petri dishes consist of glass rings attached to flat glass surfaces. Upon casting, the membrane solution was left to dry overnight at room temperature in inert N_2 atmosphere. The inert N_2 atmosphere prevented contact with the humidity in air. The vitrified membranes were peeled off carefully from the petri dish and annealed in ovens. Glass supports were used to sandwich membranes and to prevent curving. The oven was gradually heated, starting from room temperature to 100 °C (above the boiling point of $CHCl_3$), 160 °C (slightly exceeding the boiling point of DMF), 250 °C (between the boiling point of DMF, and the T*g* of Matrimid®) or 350 °C (above the T*g* of Matrimid®). Each heating step was designed to increase the temperature by 1°C/min with 50 °C increments. The oven remained isothermal for 2 hours at each increment. The membranes were kept at the final temperature for 24 hours, and subsequently removed after the oven was allowed to cool down to room temperature naturally. Immediate quenching was avoided as it is known to cause void formation between the polymer and the filler as a result of the differences in the thermal expansion coefficients. The polymer-MOF attachment was preserved by allowing the MMMs to cool down naturally.

Characterization of MMMs

Attenuated total reflectance Fourier transform infrared spectroscopy (ATR-FTIR) was carried out in air using a Varian 620 FT-IR imaging microscope with a Germanium crystal. FTIR spectra were

collected over a wavelength range from 400 to 4000 cm^{-1} with a spectral resolution of 4 cm^{-1} and 64 scans. Cross-sectional SEM imaging of the membrane was taken using a JEOL JSM-1060LV scanning electron microscope (SEM). If a membrane was sufficiently flexible, it was freeze-fractured. The membranes that were already too brittle were broken in liquid N_2. The samples were sputtered with Au/Pd for three cycles of 20 seconds in order to prevent charge build-up. Charge build-up during SEM analysis happens as a result of the non-conductive nature of the polymers, X-ray diffraction (XRD) patterns were obtained by using a Stoe-HT X-ray diffractometer, with CuKα radiation, λ=1.54 Å at room temperature. The mechanical strength of the membrane samples were tested at room temperature using a Universal Testsystem (UTS) with 0.0001 mm position resolution and load cells up to 200 N. A TA Instruments DSC Q2000 using Al hermetic closed pans and in N_2 atmosphere was used for differential scanning calorimetry (DSC) measurements. The samples were first stabilised at 20 °C for 10 minutes, then heated to 370 °C at 10 °C/minute. After 5 minutes, the samples were cooled to 20 °C at 10 °C/minute and re-heated to 370 °C as described. The thermogravimetric behaviour of samples was analysed with TA Instruments TGA-Q500. The temperature was increased from room temperature to 100 °C at 5 °C/min, maintained at this temperature for 10 minutes, then heated to 160 °C at 2 °C/min, maintained at this temperature for 10 minutes, and finally to 500 °C at 10 °C/min .The ambient atmosphere (N_2 or $O_{2,}$) is appropriately reported in the results section. The membrane samples were prepared for TEM by gluing the sample on a support to fit the holder of the microtome. It was not necessary to embed the samples in epoxy resin, as the samples consisted of polymeric membrane, The samples were then sliced with a 100 nm thickness using a Leica UC7 ultramicrotome equipped with a histo diamond knife. Selected area electron diffraction (SAED) patterns, high resolution TEM (HRTEM) and high angle annular dark field scanning TEM (HAADF-STEM) images were

acquired using a FEI Osiris microscope, operated at 200 kV. Energy dispersive X-ray spectroscopy (EDX) maps were acquired using a ChemiSTEM system, the data was analysed using the Bruker ESPRIT software.

Gas Separation

The membranes were tested for gas separation performance using binary gas mixtures. The gas separation system is a custom-built, high-throughput gas separation system (HTGS), described in detail in ref. 32. The membranes were tested at 35 °C and 10 bar cross-membrane pressure difference using a CO_2/CH_4 mixture of 50-50% vol. composition. The gas composition at the permeate side was determined using gas chromatography (GC). The membranes were first flushed with the gas mixture overnight to reach steady-state. Steady-state was confirmed by comparing consecutive GC measurements to yield the same result. Once steady-state was confirmed, three more measurements were carried out on the gas accumulated on the permeate side. The average of these three measurements was reported as a data point. Every data point was obtained from averaging the data collected from two membranes prepared from the same batch and two coupons from each membrane. The reported data for every coupon was calculated as an average of three measurements for both permeability and selectivity after steady state was reached. The MMM coupon has a surface area of 2.24 cm^2 and the active permeation area is 1.54 cm^2. The permeabilities were measured at steady-state using a constant-volume variable-pressure permeation system. The overall permeability (P_o) and the relative permeability of CO_2 (P_{CO2}) were calculated using equations as follows, respectively.[38]

$$P_o = \frac{\alpha V l}{ART\Delta P}$$

where, α represents the pressure increase rate in the permeate side with respect to time, V is the volume of the permeate side, l is the membrane thickness, A is the membrane surface area, R is the ideal gas constant, T is the permeation temperature, and ΔP is the cross-membrane pressure difference.

$$P_{CO_2} = P_o \frac{y_{CO_2}}{x_{CO_2}}$$

where, P_o refers to the overall permeability, y_{CO2} and x_{CO2} denote the CO_2 content at the permeate and feed sides, respectively.[38]

Results and Discussion

MMMs with various NH_2-MIL-53(Al) loadings (20, 30 and 40 wt%) were prepared. The as-synthesized NH_2-MIL-53(Al) filler has a particle size ranges between 300 to 600 nm according to SEM imaging (Figure S1). MMMs with different NH_2-MIL-53(Al) loadings (20-40 wt%) were prepared and thermally treated at 100, 160, 250 or 350 °C in air for periods up to 24h. The well-controlled thermal treatment at 350 °C in air induced a significant change in membrane colour, as shown in Figure 1A. The PI membrane turned from yellow to dark-brown at 350 °C, whereas the MMMs started to darken at lower temperatures already. The changes of color of the membranes from yellow to dark brown upon heat treatment at 350 °C maybe due to physicochemical changes (e.g. formation of charge transfer complexes) in the membrane during the heating. Similar observation has also been noted for other polymer membranes such as PIM-1[39] and poly(ether-block-amide) copolymer[40] membranes upon heat treatment. According to TGA (Figures 1B and S2), bulk NH_2-MIL-53(Al) starts to decompose at 200 °C. The presence of the surrounding PI-matrix significantly improved the thermal stability of the NH_2-MIL-53(Al) up to >400 °C, in line with other systems.[37] A significant weight loss before 120 °C as noted for the MMMs treated at

250 and 350 °C is due to the water formation as a result of the chain termination reaction.[41] Solubility tests after 2 days of immersion in chloroform (Figure S3) showed that the membranes treated at 160 °C were completely soluble, whereas the MMMs treated at higher temperatures had become insoluble in chloroform, showing a high gel content above 90% after 2 days (Figure S3), confirming the enhanced chemical stability.

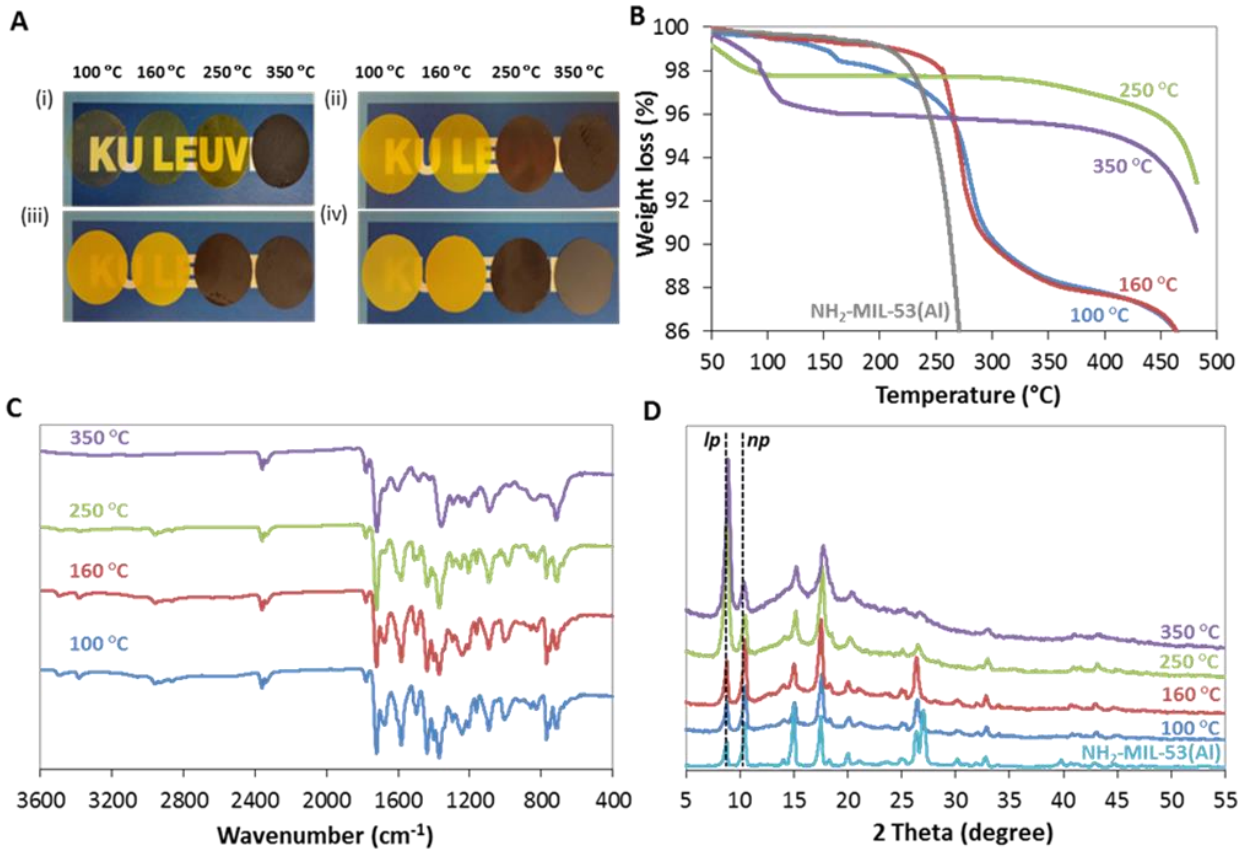

Figure 1. Solubility, Thermal, Chemical and Structural Properties of Thermally Treated MMMs. A) The change in colour of the (i) unfilled Matrimid® membranes and MMMs with different MOF loading (ii) 20 wt%, (iii) 30 wt% and (iv) 40 wt% with increasing treatment temperature. B) TGA profiles, C) FTIR spectra and D) XRD patterns of MMMs with 40 wt% NH_2-MIL-53(Al) loading treated at different temperatures in comparison to bulk NH_2-MIL-53(Al). Enlarged versions of

ATR-FTIR spectra marked with characteristic peaks assigned to thermo-oxidative crosslinking of Matrimid® and MMMs treated at different temperatures are provided in Figure S4.

The improved thermal and chemical stabilities of the MMMs confirmed the expected oxidative PI-crosslinking.[37] In order to confirm this phenomenon and to provide insight into the interactions between the polymer and the embedded MOF, the MMMs were characterized by ATR-FTIR (Figures 1C and S4). Oxidative crosslinking of Matrimid® occurs through the C-H groups is confirmed according to the observed reduction in intensity of the characteristic bands corresponding to the aliphatic C-H stretching (2954, 2921 and 2860 cm^{-1}) (Figure S4). The thermally-induced oxidative crosslinking of the polymer due to the combination of radical sites on adjacent chains has been previously discribed in detail.[37]

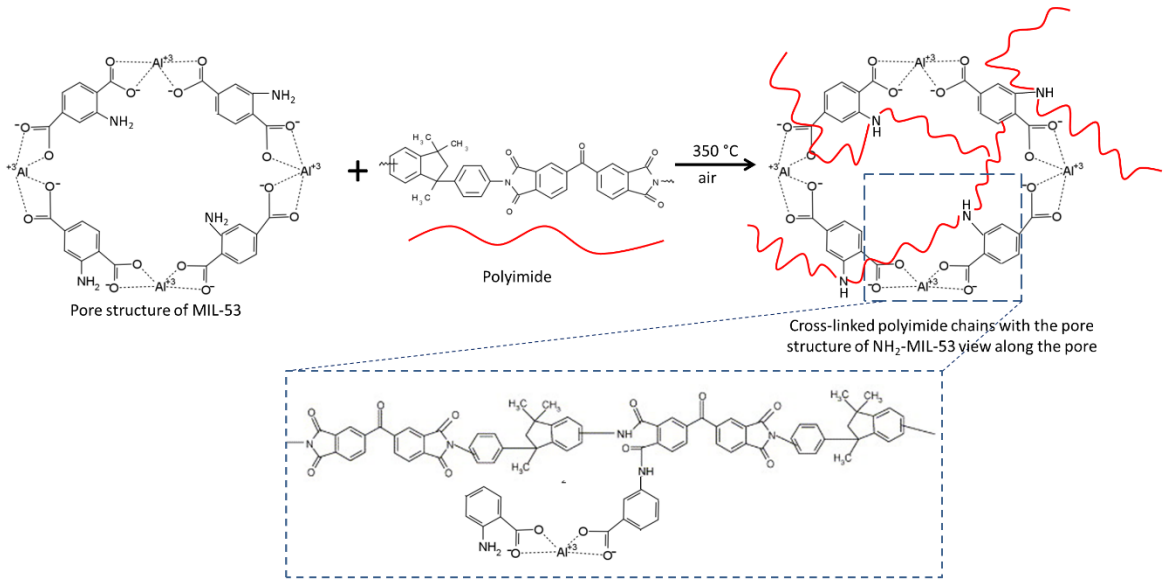

Scheme 1. Schematic showing the mechanism of chemical crosslinking of polyimide polymer chains with the amino functions at the pore entrance of NH_2-MIL-53(Al) upon thermal treatment at 350 °C in air.

The bands at 1774 and 1716 cm^{-1} are assigned to the symmetric and asymmetric stretching of the C=O groups of the polymer imide (Figure S4).[42] The 1365 cm^{-1} absorption band is attributed to the C−N stretching of the imide five-membered ring of the polyimide membrane. The crosslinking of amino functions (NH_2-MIL-53) with the polymer chains at the pore mouth is confirmed via the appearance of the amide signals at 1538 cm^{-1} which is attributed to N−H bending and the disappearance of the two bands at 3352 and 3482 cm^{-1} related to the symmetric and asymmetric vibrations of NH_2 groups of NH_2-MIL-53(Al), respectively.[42,43] Also, the transverse stretching of C–N–C at 1084 cm^{-1} which characterizes the presence of the imide groups were also found to decrease. However, the intensity of these absorption bands are not significant mainly due to the relatively low concentration of formed amide groups between the MOF particles and polymer matrix at the interface as only the terminal amino functions at the outer surface of the MOFs will take part for this specific crosslinking reaction. Similar observations of polyimide-MOF interaction has also been reported.[42,43] The crosslinking process is initiated by the attack of the imide functional groups of Matrimid® at the amino groups of the bridging terephthalates,[44] most probably occurs at the pore mouth. (Scheme 1). The PI-bulk crosslinking and the reduced chain mobility at the MOF-polymer interface were directly reflected in the Tg of the membranes,[45] where an increase in the Tg values from 318 to 326, 328 and 337 °C were noted with 20, 30 and 40 wt% loading, respectively. Similarly, the tensile strength of the membranes was also induced as the crosslinking temperature increases, as shown in the Table S1 and Figure S5.

XRD patterns of the MMMs (Figures 1D and S6-S9) reveal that the structure of MIL-53 was preserved, despite a sign of crystallinity loss, after treatment at 350 °C. It was noted from the TG analyses that the MMMs treated at high temperatures (250 and 350 °C) exhibit an enhanced thermal stability up to 400 °C, whereas the MMMs annealed at lower temperatures (160 and 100

°C) start to decompose at 200 °C. Similar thermal behaviour was observed for bulk NH_2-MIL-53(Al). The results suggest that the thermal cross-linking significantly enhanced the thermal stability of the NH_2-MIL-53(Al) embedded in the polymer matrix. NH_2-MIL-53(Al) is a flexible MOF.[25,46,47] The removal of the trapped molecules triggers the direct structural change from either the *np* form (*np* guest such as H_2O) or the *lp* form (*lp* guest such as DMF and terephthalic acid) to the empty *lp* form upon activation above 100 °C. This material transforms to the *np* phase after cooling under ambient conditions due to adsorption of water molecules. Adsorption of CO_2 could also induce the transition from the *lp* to the *np* form. However, for the case of NH_2-MIL-53(Al) in its hydrated form, CO_2 adsorption at low pressures only produces minor structural changes due to stronger hydrogen-bonds interaction in the framework structure.[25,47] Only at higher partial pressure above 10 bar, the *np* form will expand to its *lp* form.[47] This observation was further confirmed by XRD (Figure 1D), showing exclusively the *np* configuration for bulk NH_2-MIL-53(Al) and the MMMs treated at low temperature (100 and 160 °C). Interestingly, the embedded NH_2-MIL-53(Al) in the polymer matrix showed the *lp* form after heating the MMM above 160 °C.[48-50] Although such transition normally occurs in presence of penetrants, such as DMF[50] or CO_2,[51] in the MOF pores, the FTIR (Figures 1C and S4) and TGA results (Figures 1B and S2) however, confirm the absence of any adsorbed species. The lack of FTIR signals in the 1673–1690 cm^{-1} range, assigned to the amide group of the DMF, indeed indicates that the MOF was well-washed and solvent exchanged with methanol and chloroform. Moreover, the TGA curves do not exhibit any observable weight loss around the boiling point of DMF (153 °C). The *np* form of NH_2-MIL-53(Al) is energetically preferred over the *lp* form. Hence, the *np* form should prevail again after cooling down. The expanded MOF framework in the MMMs is however retained, as evidenced by the XRD patterns. Such observation can be ascribed to the (at least partial) penetration and

chemical fixation of the PI chains in the NH_2-MIL-53(Al) pores. As proven above, covalent bonding between the polymer and the amino functions on the pore walls takes place at these high temperatures, thus leaving no possibility for the MOF-structure to relax again upon cooling. Penetration of polymer chains into the *lp* pore can be characterized by the glass transition temperature (Tg).[52] For the 40 wt% NH_2-MIL-53(Al) loaded MMM treated at 100 °C, in which the NH_2-MIL-53(Al) has the *np* form, the measured Tg was 318 °C. For the 40 wt% NH_2-MIL-53(Al) loaded MMM treated at 350 °C, in which the NH_2-MIL-53(Al) has an *lp* form, the measured Tg was 337 °C. A significant 19 °C increase in Tg temperature is indicative for polymer penetration into the open pore structure of NH_2-MIL-53(Al). A similar observation has also been reported for the penetration of polymer chains into the open pore structure of MIL-53[52] and mesoporous ZSM-5[53] loaded Matrimid membranes. Direct evidence of polymer chain penetration into the pore structure of UiO-66 embedded in the polymer matrix has also been confirmed by solid-state NMR studies[54] and molecular simulations.[55]

Figure S10 shows the cross-sectional SEM images of unfilled PI membranes and MMMs with 20, 30 and 40 wt% loading. The unfilled PI membranes do not show observable change in morphology with increasing treatment temperature. For MMMs, the NH_2-MIL-53(Al) (light regions) and polymer (dark regions) can be clearly identified by the contrast between the two nanostructure phases. With the present MIL-53-Matrimid® system, the polymer and the MOF create a perfectly homogeneous MMM even at high MOF loading. When the MMMs were thermally treated at 350 °C, thus surpassing the T*g* of Matrimid® (~305 °C) under controlled heating and cooling, the polymer chains are expected to adhere much better to the surface of the MOF particles, considering the chemical nature of the MOF linker which shows many possibilities for physico-chemical interactions with the PI chain (e.g. π-stacking and H-bonding).[56,57]

Interfacial voids at grain boundaries in MMMs are detrimental to membrane selectivity. They are created by poor polymer-filler interactions and are frequently encountered in MMMs, especially at high loadings.[58] A combination of high angle annular dark field scanning transmission electron microscopy (HAADF-STEM), selected area electron diffraction (SAED) and energy dispersive X-ray (EDX) analysis was performed in order to provide insight into the

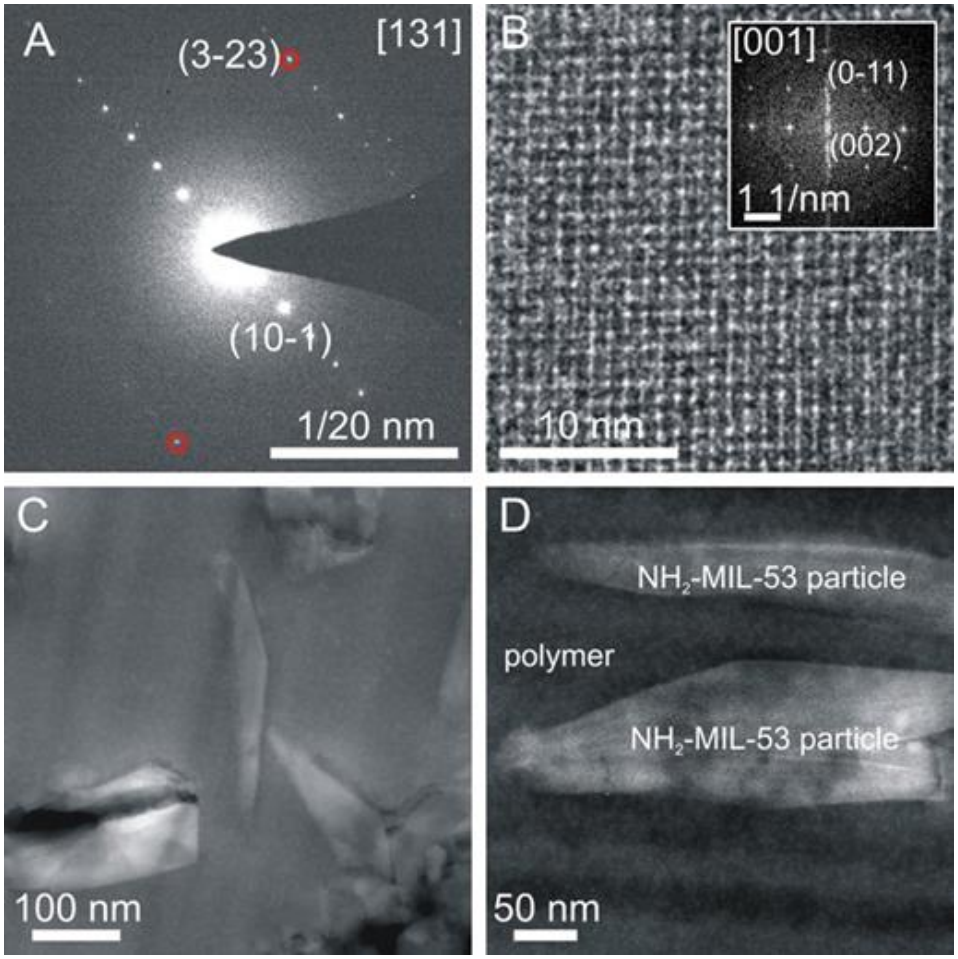

Figure 2. Advanced TEM characterization of MMM with 40 wt% NH_2-MIL-53(Al) Loading. A) SAED pattern recorded along [131] zone axis from NH_2-MIL-53(Al) nanoparticle. B) HRTEM

micrograph and corresponding FFT pattern from a similar particle as in (A). C and D) HAADF-STEM image displaying the morphology of NH_2-MIL-53(Al) particles embedded in a MMM.

compatibility of the MOF with the PI as well as the crystallinity of the embedded NH_2-MIL-53(Al). The results confirm that the crystallinity of the incorporated NH_2-MIL-53(Al) is preserved (Fig. 2A). Since the structure and morphology of the fillers change quickly under electron beam irradiation, a low dose electron beam was selected to record reliable diffraction data. Figure 2B displays an HRTEM micrograph acquired from a similar particle along the [001] zone axis. The measured *d*-values and diffraction angles from the SAED pattern are in strong agreement with the known orthorhombic *lp* form structure model (space group: *Imma)*, in full agreement with the XRD results (Figure 1D) and as reported elsewhere.[59] An overview of HAADF-STEM images depicting the morphology of the particles embedded inside the MMM is presented in Fig. 2C and 2D. The TEM images (Figures 2C and 2D) reveal excellent compatibility at the filler-PI interface. The blue arrows indicate a dark contrast at the interface between the particles and the MMM, mainly due to cutting artefacts during the sample preparation. The chemical distribution of the individual Al and O elements visualized by EDX mapping (Figures S10B and S10C) was acquired from the red highlighted region in Figure S11A, confirming the presence of incorporated NH_2-MIL-53(Al) in the polymer matrix.

Figure 3 and Table S2 show the mixed-gas permselectivity as a function of the heat treatment temperature for unfilled Matrimid® and MMMs with different loadings. The CO_2/CH_4 selectivity increases with increasing filler loadings. Especially at the maximal loading (40 wt%), a high CO_2/CH_4 selectivity of 153 was achieved without sacrificing much CO_2 permeability. To

investigate the accessibility of the MMM by the permeating gas, single CO_2 adsorption isotherms were measured of the MMMs with 40 wt% MOF loading treated at different temperatures (Figure S12). The isotherms revealed that the composite membranes are accessible to CO_2. However, it should be noted that the accessibility of MMMs to CO_2 adsorption is reduced particularly upon

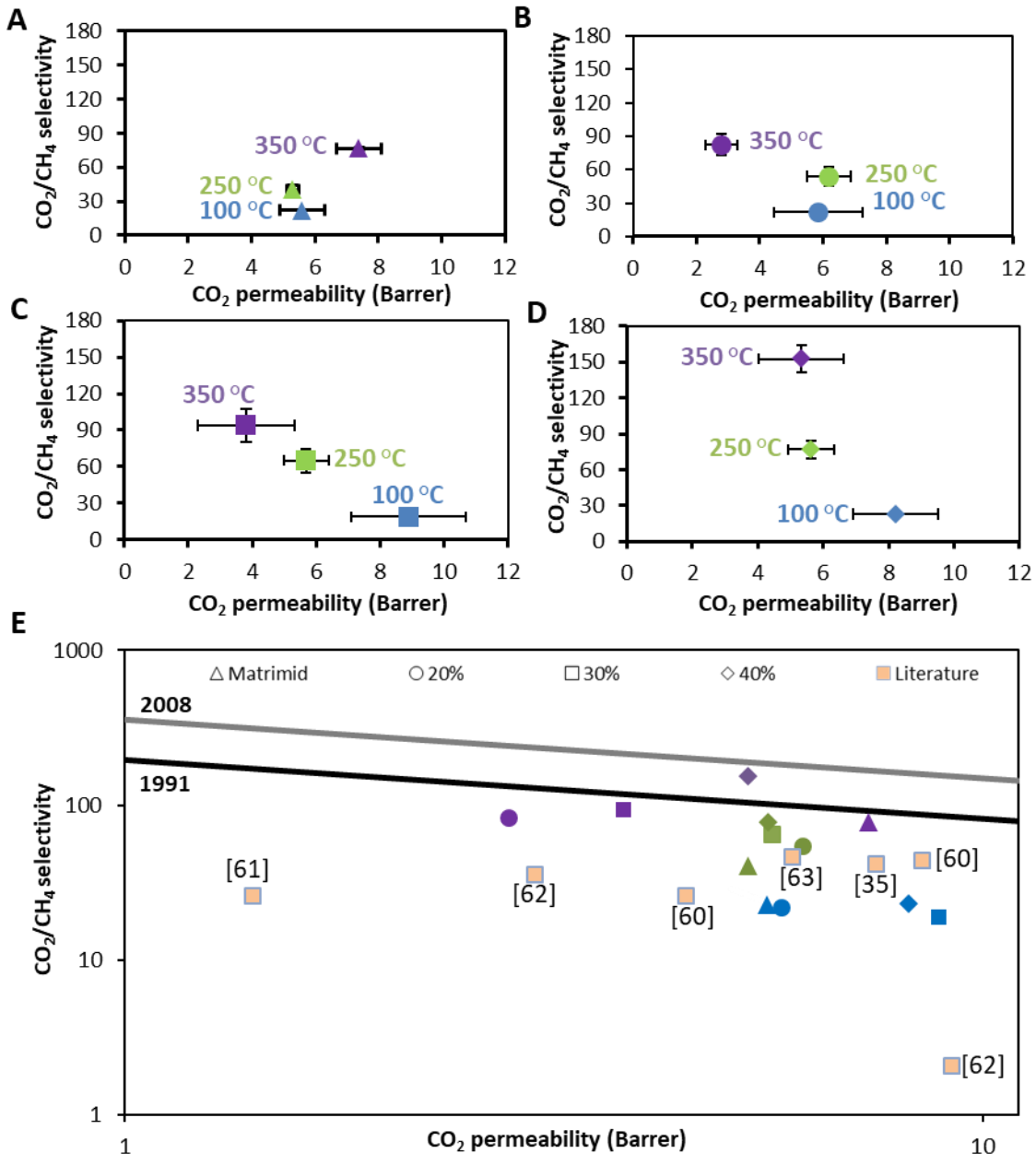

Figure 3. The Evolution of the separation performance of the thermally treated membranes. A)

Matrimid® and B-D) MMMs with 20, 30 and 40 wt% NH_2-MIL-53(Al) loading treated at increasing annealing temperature. E) The Robeson plot of 1991 and 2008 compared with the results from literature (orange squares), and results obtained from this work (blue: 100 °C; green: 250 °C and purple: 350 °C). A detailed comparison of all MOF loaded MMMs results with all MOF-loaded MMM together with the measurement conditions is presented in Table S2.

thermal treatment at 350 °C mainly due to densification of the composite membranes as a result of polymer-polymer and polymer-filler crosslinking, in full agreement with the gas separation results. It should be mentioned that the unfilled Matrimid® membranes treated at 100 °C only show a CO_2/CH_4 selectivity of 22 under similar conditions (Table S2). The results suggest that a relatively high filler loading is required in order to maximally gain from the effect of incorporating MOF crystals in the PI matrix. In most other cases,[64] selectivities start to drop significantly at these higher loading due to creation of defects, proving again the excellent MOF-PI interactions realized here. In order to study whether the enhanced selectivity achieved from the crosslinked MMMs was due to surface effects, NH_2-MIL-53(Al) nanoparticles having an average particle size of 50 nm (Fig. S13) were synthesized according to the recipe reported by Wu *et al.*[65] MMMs with 10 wt% loading of NH_2-MIL-53(Al) nanoparticles were prepared and treated at 350 °C. Gas separation results showed that the MMMs incorporated with NH_2-MIL-53(Al) nanoparticles did not show improvements in CO_2/CH_4 selectivity. In contrast, CO_2/CH_4 selectivity decreased and CO_2 permeability increased (Table S2). It is likely that the smaller particles tend to agglomerate and create interfacial gaps/voids when dispersed into the polymer matrix, resulting in non-selective gas transport pathways, despite efforts to better disperse the non-dried NH_2-MIL-53(Al) nanoparticles via sonication prior to MMM preparation. SEM imaging of the NH_2-MIL-53(Al)

nanoparticle loaded MMM cross-section is shown in Fig. S14. Agglomerations and interfacial gaps are observed throughout the MMM. These results suggest that the particle size of the fillers does play a crucial role in its dispersion in the polymer. Large agglomeration of the particles within the polymer interact poorly with the polymer, resulting in non-selective defects. Similar issue has also been encountered and reported for MMM loaded with nanosized MOF-74,[66] ZIF-8[67] and NH_2-MIL-53.[68] For example, the preparation of MMMs based on polybenzimidazole (PBI) and ZIF-8 nanoparticles of different average sizes (50, 70 and 150 nm) has been documented.[67] According to the gas separation results, both permeability and selectivity of the MMMs were dramatically reduced as the filler size decreased, due to the higher degree of nanoparticle agglomeration owing to their higher external surface area. Similarly, particles agglomeration has also been reported on the top layer of MMMs prepared from 100 nm-sized NH_2-MIL 53(Al) filler even at low filler loading (10 wt%).[68] Therefore, in some cases (depending on MOF type), agglomeration of MOF filler in the polymer matrix could not be avoided despite nanosized MOF fillers are used for the fabrication of MOF-based MMMs.

The pore dimensions of NH_2-MIL-53(Al) (7.5 Å) are far larger than the kinetic diameters of CO_2 (3.3 Å) and CH_4 (3.8 Å),[31] which is contradicting the outstanding selectivities achieved for the highly loaded MMMs.[36] The selectivity increase thus has to be fully ascribed to the partial blockage of the pore mouths by the penetrated polymer chains and the densified matrix around it.[36,58] NH_2-MIL-53 crystals were reported to transform to two main possible conformations that can be distinguished: the *lp* and *np* forms when activated at different temperature,[52] which is in full agreement with our XRD data as presented in Figure 1D. Accordingly to our results (Figure 1D), *lp* form is obtained when the NH_2-MIL-53(Al) loaded MMMs were treated at 250 and 350 °C, whereas the *np* form is obtained when the NH_2-MIL-53(Al) loaded MMMs were treated at 100

and 160 °C. From the gas separation point of view, gas transport would have been enhanced with NH_2-MIL-53(Al) in its *lp* form in the MMM but the selectivity would have decreased. While in its *np* form NH_2-MIL-53(Al) would serve as a selective molecular sieve to give high CO_2/CH_4 selectivity. At the same time CO_2 permeability would decrease. In this work, we demonstrate that the penetration of the polymer chains into the pores of NH_2-MIL-53(Al) could maintain its *lp* configuration. Coupled with the simultaneous polymer-polymer crosslinking in the bulk of the membrane, a network that is sufficiently dense to hinder the permeation of CH_4 is thus formed as illustrated by the very limited sacrifices in CO_2 permeability that accompany this exceptional improvement in selectivity, contrasting earlier work with comparable systems.[37] This very modest reduction in CO_2 permeability is possible thanks to the fact that only MOF pore entrances were crosslinked by the polymer chains, thus retaining the *lp* form.

A major drawback for membrane-based gas separations is the loss in selectivity that is often encountered as a result of excessive polymer mobility due to interaction with CO_2 at high feed pressure. The crosslinked MMM with 40 wt% MOF loading was therefore evaluated for its plasticization resistance at high feed pressure (40 bar). The gas separation measurement performed at 40 bar confirmed that the crosslinked MMM could retain its high CO_2/CH_4 selectivity (Table S3). It is also important to mention that early research in this field has reported about the issue of embrittlement in MOF-loaded MMMs when MOF loading increases.[69] The MMMs will become brittle when the filler loading increases to > 30 wt%. At a very high filler loadings (60 wt%), the MMMs were not selective for CO_2/CH_4 separation.[70] However, according to the measured mechanical properties of our MMMs treated at different temperatures (100-350 °C), the tensile strength of the MMMs with 40 wt% loading increases from 24.5 to 32.7 MPa with increasing temperature from 100 to 350 °C as shown in Table S1 and Figure S5 which can be explained from

the observed membrane densification as a result of crosslinking. Although the MMMs with 40 wt% loading showed a sign of brittleness in comparison to the unfilled polyimide membranes, the fabricated MMMs with 40 wt% MOF loading and thermally treated at 350 °C could still survive at pressure up to 10 bar and gave promising CO_2/CH_4 selectivity (Figure 4D).

The position of a polymer's gas permeability data relative to the Roberson upper bound is used as the universal performance indicator for assessing its potential for the separation of CO_2 from CH_4, as depicted in Figure 3E.[9] Figure 3E and Table S2 show the CO_2/CH_4 selectivities and CO_2 permeabilities for the presented MMMs compared to other NH_2-MIL-53(Al) loaded MMMs obtained from literature. The MMM treated at 350 °C with 40 wt% loading achieved the highest mixed-gas CO_2/CH_4 selectivity of 153 with a CO_2 permeability of 5.8 Barrer (purple circles), and hit the 2008 upper-bound, clearly outperforming the unfilled Matrimid® membranes (blue diamonds) and earlier reported NH_2-MIL-53(Al) loaded MMMs (orange squares). These crosslinked MMMs also reached the state-of-the-art separation performances of MMMs based on commercially available polymers embedding other MOF-types (Table S3).[19]

Conclusions

In summary, NH_2-MIL-53(Al) loaded MMMs with excellent MOF dispersion and polymer-MOF adhesion were prepared. As a result of thermal treatment at 350 °C, the physiochemical properties e.g. solubility, density, glass transition temperature and mechanical strength of the thermally treated MMMs were enhanced. Treatment of the MMMs at high temperatures induced thermo-oxidative crosslinking of the PI matrix, as well as the covalent bonding between the polymer and the NH_2 groups at the MOF pore mouth. During the thermal treatment, the MOF underwent a configurational transition from its *np* to *lp* form, which allowed the polymer chains to partially penetrate and crosslink to the amine groups at the entrance of the MOF pores. The anchoring of

the PI-chains forced the MOF to retain its *lp* form. As a result, very high mixed gas CO_2/CH_4 selectivities were thus realized without sacrifying too much permeability. These crosslinked MMMs show exciting potential for purification of biogas and natural gas, but also for use in liquid and other gas phase separations.

ASSOCIATED CONTENT

Supporting Information.

Supplemental Information includes characterization of MOF, PI and mixed-matrix membranes by SEM (Figures S1, S10, S13, S14), TGA (Figure S2), solubility test (Figure S3), ATR-FTIR (Figure S4), tensile strength (Figure S5 and Table S1)), XRD (Figures S6-S9), TEM (Figure S11), CO_2 adsorption isotherms (Figure S12) and gas separation results (Tables S2-3).

The following files are available free of charge.

Supporting Information (PDF)

AUTHOR INFORMATION

Corresponding Author

* E-mail: likhong.wee@kuleuven.be; ivo.vankelecom@kuleuven.be

Present Addresses

[†]Adsorption & Advanced Materials, Department of Chemical Engineering and Biotechnology, University of Cambridge, West Cambridge Site, Philippa Fawcett Drive, Cambridge, CB3 OAS, United Kingdom

Author Contributions

A.K. executed the experiments including material synthesis, membrane fabrication, characterization and gas separation evaluation. L.H.W. directed the membrane characterization and analyzed all the data. K.S. acquired and analyzed the TEM results in the supervision of S.B. A.K. wrote the first draft of the manuscript and completed by L.H.W. with input from all authors. I.F.J.V. initiated the project and obtained the funding. L.H.W. and I.F.J.V. supervised the project.

Notes

The authors declare no competing financial interest.

ACKNOWLEDGMENT

A.K. is grateful to the Erasmus Mundus Doctorate in Membrane Engineering (EUDIME) programme. L.H.W. thanks the FWO-Vlaanderen for a postdoctoral research fellowships under contract number 12M1418N. The authors would like to thank Methusalem and IAP-PAI for research funding. S.B. acknowledges financial support from European Research Council (ERC) (ERC Starting Grant No. 335078-COLOURATOM). We are also grateful to Frank Mathijs (KU Leuven) for the mechanical tests, Bart Goderis and Olivier Verkinderen for the DSC measurements and Huntsman (Switzerland) for providing the Matrimid® polymer.

REFERENCES

1. Baker, R.W.; Lokhandwala, K. Natural Gas Processing with Membranes: An Overview. Ind. Eng. Chem. Res. **2008**, *47*, 2109–2121.

2. Baker, R. W. *Membrane Technology and Applications*, John Wiley & Sons Ltd., Chichester, UK, 2012; pp. 1–14.

3. Tanaka, K.; Okamoto, K. -I. *Materials Science of Membranes for Gas and Vapor Separation*, Yampolskii, Y., Pinnau, I., Freeman B., Eds., John Wiley & Sons Ltd, Chichester, UK, 2006; pp. 271–291.

4. Bachman, J. E.; Long, J. R. Plasticization-resistant Ni_2(dobdc)/polyimide Composite Membranes for the Removal of CO_2 from Natural Gas. Energy Environ. Sci. **2016**, *9*, 2031–2036.

5. Thornton, A. W.; Dubbeldam, D.; Liu, M. S.; Ladewig, B. P.; Hill, A. J.; Hill, M. R. Feasibility of Zeolitic Imidazolate Framework Membranes for Clean Energy Applications. Energy Environ. Sci. **2012**, *5*, 7637-7646.

6. Makaruk, A.; Miltner, M.; Harasek, M. Membrane Biogas Upgrading Processes for the Production of Natural Gas Substitute. Sep. Purif. Technol. **2010**, *74*, 83–92.

7. Scholz, M.; Melin, T.; Wessling, M. Transforming Biogas into Biomethane using Membrane Technology. Renew. Sustain. Energy Rev. **2013**, *17*, 199–212.

8. Robeson, L. M. Correlation of Separation Factor versus Permeability for Polymeric Membranes. J. Membr. Sci. **1991**, *62*, 165–185.

9. Robeson, L. M. The Upper Bound Revisited. J. Membr. Sci. **2008**, *320*, 390–400.

10. Hillock, A. M. W.; Miller, S. J.; Koros, W. J. Crosslinked Mixed Matrix Membranes for the Purification of Natural Gas: Effects of Sieve Surface Modification. J. Membr. Sci. **2008**, *314*, 193–199.

11. Wind, J. D.; Paul, D. R.; Koros, W. J. Natural Gas Permeation in Polyimide Membranes. J. Membr. Sci. **2004**, *228*, 227–236.

12. Cao, C.; Chung, T. -S.; Liu, Y.; Wang, R.; Pramod, K. P. Chemical Cross-linking Modification of 6FDA-2, 6-DAT Hollow Fiber Membranes for Natural Gas Separation J. Membr. Sci. **2003**, *216*, 257–268.

13. Chung, T. -S.; Jiang, L.; Li, Y.; Kulprathipanja, S. Mixed Matrix Membranes (MMMs) Comprising Organic Polymers with Dispersed Inorganic Fillers for Gas Separation. Prog. Polym. Sci. **2007**, *32*, 483–507.

14. Mahajan, R.; Koros, W. J. Factors Controlling Successful Formation of Mixed-matrix Gas Separation Materials. Ind. Eng. Chem. Res. **2000**, *39*, 2692–2696.

15. Sudhir, S. K.; David J. H.; David R. C. Aspi N. P. Gas Separation Membrane with Organosilicon-treated Molecular Sieve. U.S. Patent 6508860B1, January 21, 2003.

16. Guiver, M. D.; Thi, H. N. L.; Robertson, G. P. Composite gas separation membranes. U.S. Patent 6605140. August 12, 2003.

17. Wang, S.; Wu, Y.; Zhang, N.; He, G.; Xin, Q.; Wu, X.; Wu, H.; Cao, X.; Guiver, M. D.; Jiang, Z. A Highly Permeable Graphene Oxide Membrane with Fast and Selective Transport Nanochannels for Efficient Carbon Capture. Energy Environ. Sci. **2016**, *9*, 3107–3112.

18. Jiang, X.; Li, S.; He, S.; Bai, Y.; Shao, L. Interface Manipulation of CO_2–philic Composite Membranes Containing Designed UiO-66 Derivatives Towards Highly Efficient CO_2 Capture. J. Mater. Chem. A **2018**, *6*, 15064–15073.

19. Jiang, X.; Li, S.; Bai, Y.; Shao, L. Ultra-facile Aqueous Synthesis of Nanoporous Zeolitic Imidazolate Framework Membranes for Hydrogen Purification and Olefin/Paraffin Separation. J. Mater. Chem. A **2019**, *7*, 10898–10904.

20. Li, J. -R.; Kuppler, R. J.; Zhou, H. -C. Selective Gas Adsorption and Separation in Metal–organic Frameworks. Chem. Soc. Rev. **2009**, *38*, 1477–1504.

21. Seoane, B.; Coronas, J.; Gascon, I.; Benavides, M. E.; Karvan, O.; Caro, J.; Kapteijn, F.; Gascon, J. Metal–organic Framework Based Mixed Matrix Membranes: A Solution for Highly Efficient CO_2 Capture? Chem. Soc. Rev. **2015**, *44*, 2421–2454.

22. Férey, G. Hybrid Porous Solids: Past, Present, Future. Chem. Soc. Rev. **2008**, *37*, 191–214.

23. Férey, G.; Serre, C. Large Breathing Effects in Three-dimensional Porous Hybrid Matter: Facts, Analyses, Rules and Consequences. Chem. Soc. Rev. **2009**, *38*, 1380–1399.

24. Alhamami, M.; Doan, H.; Cheng, C. -H. A Review on Breathing Behaviors of Metal-organic-Frameworks (MOFs) for Gas Adsorption. Materials **2014**, *7*, 3198–3250.

25. Stavitski, E.; Pidko, E. A.; Couck, S.; Remy, T.; Hensen, E. J. M.; Weckhuysen, B. M.; Denayer, J.; Gascon, J.; Kapteijn, F. Complexity Behind CO_2 Capture on NH_2-MIL-53(Al). Langmuir **2011**, *27*, 3970–3976.

26. Liu, Y.; Her, J. -H.; Dailly, A.; Ramirez-Cuesta, A. J.; Neumann, D. A.; Brown, C. M. Reversible Structural Transition in MIL-53 with Large Temperature Hysteresis. J. Am. Chem. Soc. **2008**, *130*, 11813–11818.

27. Salles, F.; Ghoufi, A.; Maurin, G.; Bell, R. G.; Mellot-Draznieks, C.; Férey, G. Molecular Dynamics Simulations of Breathing MOFs: Structural Transformations of MIL-53(Cr) upon Thermal Activation and CO_2 Adsorption. Angew. Chem. Int. Ed. **2008**, *120*, 8487–8491.

28. Trung, T. K.; Trens, P.; Tanchoux, N.; Bourrelly, S.; Llewellyn, P. L.; Loera-Serna, S.; Serre, C.; Loiseau, T.; Fajula, F.; Férey, G. Hydrocarbon Adsorption in the Flexible Metal Organic Frameworks MIL-53(Al, Cr). J. Am. Chem. Soc. **2008**, *130*, 16926–16932.

29. Llewellyn, P. L.; Bourrelly, S.; Serre, C.; Filinchuk, Y.; Férey, G. How Hydration Drastically Improves Adsorption Selectivity for CO_2 over CH_4 in the Flexible Chromium Terephthalate MIL-53. Angew. Chem. Int. Ed. **2006**, *45*, 7751–7754.

30. Zhang, F.; Zou, X.; Gao, X.; Fan, S.; Sun, F.; Ren, H.; Zhu, G. Hydrogen Selective NH_2-MIL-53(Al) MOF Membranes with High Permeability. Adv. Funct. Mater. **2012**, *22*, 3583–3590.

31. Couck, S.; Rémy, T.; Baron, G. V.; Gascon, J.; Kapteijn, F.; Denayer, J. F. M. A Pulse Chromatographic Study of the Adsorption Properties of the Amino-MIL-53 (Al) Metal–organic Framework. Phys. Chem. Chem. Phys. **2010**, *12*, 9413–9418.

32. Boutin, A.; Couck, S.; Coudert, F. X.; Serra-Crespo, P.; Gascon, J.; Kapteijn, F.; Fuchs, A.H.; Denayer, J. F. M. Thermodynamic Analysis of the Breathing of Amino-functionalized MIL-53(Al) upon CO_2 Adsorption. Micropor. Mesopor. Mater. **2011**, *140*, 108–113.

33. Rodenas, T.; Luz, I.; Prieto, G.; Seoane, B.; Miro, H.; Corma, A.; Kapteijn, F.; Llabrés i Xamena, F. X.; Gascon, J. Metal-organic Framework Nanosheets in Polymer Composite Materials for Gas Separation. Nature Mater. **2015**, *14*, 48–55.

34. Qilei Song, S. K. Nataraj, Mina V. Roussenova, Jin Chong Tan, David J. Hughes, Wei Li, Pierre Bourgoin, M. Ashraf Alam, Anthony K. Cheetham, Shaheen A. Al-Muhtaseb and Easan Sivaniah. Zeolitic imidazolate framework (ZIF-8) based polymer nanocomposite membranes for gas separation ***Energy Environ. Sci.***, 2012,**5**, 8359-8369

35. Sabetghadam, A.; Seoane, B.; Keskin, D.; Duim, N.; Rodenas, T.; Shahid, S.; Sorribas, S.; Le Guillouzer, C.; Clet, G.; Tellez, C.; Daturi, M.; Coronas, J.; Kapteijn, F.; Gascon, J. Metal Organic Framework Crystals in Mixed-matrix Membranes: Impact of the Filler Morphology on the Gas Separation Performance. Adv. Funct. Mater. **2016**, *26*, 3154–3163.

36. Rodenas, T., van Dalen, M., García-Pérez, E., Serra-Crespo, P., Zornoza, B., Kapteijn, F., and Gascon, J. (2014). Visualizing MOF mixed matrix membranes at the nanoscale: Towards structure-performance relationships in CO_2/CH_4 separation over NH_2-MIL-53(Al)@PI. Adv. Funct. Mater. *24*, 249-256.

37. Kertik, A.; Wee, L. H.; Pfannmöller, M.; Bals, S.; Martens, J. A.; Vankelecom, I. F. J. Highly Selective Gas Separation Membrane using In Situ Amorphised Metal–organic Frameworks. Energy Environ. Sci. **2017**, *10*, 2342–2351.

38. Khan, A. L.; Basu, S.; Cano-Odena, A.; Vankelecom, I. F. J. Novel High Throughput Equipment for Membrane-based Gas Separations. J. Membr. Sci. **2010**, *354***,** 32–39.

39. Song, Q.; Cao, S.; Pritchard, R. H.; Ghalei, B.; Al-Muhtaseb, S. A.; Terentjev, E. M.; Cheetham, A. K.; Sivaniah, E. Controlled Thermal Oxidative Crosslinking of Polymers of Intrinsic Microporosity Towards Tunable Molecular Sieve Membranes. Nature Commun. **2014**, *5*, 4813.

40. Martínez-Izquierdo, L.; Malankowska, M.; Sánchez-Laínez, J.; Téllez, C.; Coronas, J. Poly(ether-block-amide) Copolymer Membrane for CO_2/N_2 Separation: The Influence of the Casting Solution Concentration on Its Morphology, Thermal Properties and Gas Separation Performance. R. Soc. open sci. **2019**, *6*, 190866.

41. Kuroda, S.; Mita, I. Degradation of Aromatic Polymers—II. The Crosslinking during Thermal and Thermo-oxidative Degradation of a Polyimide. Eur. Polym. J. **1989**, *25***,** 611–620.

42. Anjum, M. W.; Vermoortele, F.; Khan, A. L.; Bueken, B.; De Vos, D. E.; Vankelecom, F. J. Modulated UiO-66-Based Mixed-Matrix Membranes for CO_2 Separation. *ACS Appl. Mater. Interfaces* **2015**, 7, 25193-25201.

43. Tin, P. S.; Chung, T. S.; Liu, Y.; Wang, R.; Liu, S. L.; Pramoda, K. P. Effects of Cross-linking Modification on Gas Separation Performance of Matrimid Membranes. J. Membr. Sci. **2003**, *225*, 77–90.

44. Toh, Y. H. S.; Lim, F. W.; Livingston, A. G. Polymeric Membranes for Nanofiltration in Polar Aprotic Solvents. J. Membr. Sci. **2007**, *301*, 3–10.

45. Nielsen, L. E. Cross-linking Effect on Physical Properties of Polymers. J. Macromol. Sci. Part C Polym. Rev. **1969**, *3*, 69–103.

46. Schneemann, A.; Bon, V.; Schwedler, I.; Senkovska, I.; Kaskel, S.; Fischer, R. A. Flexible Metal–organic Frameworks. Chem. Soc. Rev. **2014**, *43*, 6062–6096.

47. Llewellyn, P. L.; Bourrelly, S.; Serre, C.; Filinchuk, Y.; Férey, G. How Hydration Drastically Improves Adsorption Selectivity for CO_2 over CH_4 in the Flexible Chromium Terephthalate MIL-53. Angew. Chem. Int. Ed. **2006**, *45*, 7751–7754.

48. Goesten, M. G.; Gupta, K. B. S. S.; Ramos-Fernandez, E. V.; Khajavi, H.; Gascon, J.; Kapteijn, F. Chloromethylation as a Functionalisation Pathway for Metal–organic Frameworks. CrystEngComm **2012**, *14*, 4109–4111.

49. Cheng, X.; Zhang, A.; Hou, K.; Liu, M.; Wang, Y.; Song, C.; Zhang, G.; Guo, X. Size- and Morphology-controlled NH_2-MIL-53(Al) Prepared in DMF–water Mixed Solvents. Dalton Trans. **2013**, *42*, 13698–13705.

50. Serra-Crespo, P.; Gobechiya, E.; Ramos-Fernandez, E. V.; Juan-Alcañiz, J.; Martinez-Joaristi, A.; Stavitski, E.; Kirschhock, C. E. A.; Martens, J. A.; Kapteijn, F.; Gascon, J. Interplay of Metal Node and Amine Functionality in NH_2-MIL-53: Modulating Breathing Behavior through Intra-framework Interactions. Langmuir **2012**, *28*, 12916-12922.

51. Seoane, B.; Téllez, C.; Coronas, J.; Staudt, C. NH_2-MIL-53(Al) and NH_2-MIL-101(Al) in Sulfur-containing Copolyimide Mixed Matrix Membranes for Gas Separation. Sep. Purif. Technol. **2013**, *111*, 72–81.

52. Hsieh, J. O.; Balkus Jr. K. J.; Ferraris, J. P.; Musselman, I. H. MIL-53 Frameworks in Mixed-matrix Membranes. Micropor. Mesopor. Mater. **2014**, *196*, 1651–74.

53. Zhang, Y.; Balkus Jr. K. J.; Musselman, I. H.; Ferraris, J. P. Mixed-matrix Membranes Composed of Matrimid® and Mesoporous ZSM-5 Nanoparticles. J. Membr. Sci. **2008**, *325*, 28–39.

54. Duan, P.; Moreton, J. C.; Tavares, S. R.; Semino, R.; Guillaume Maurin, G.; Cohen, S. M.; Schmidt-Rohr, K. Polymer Infiltration into Metal–Organic Frameworks in Mixed-Matrix Membranes Detected in Situ by NMR. J. Am. Chem. Soc. **2019**, *141*, 18, 7589–7595.

55. Semino, R.; Moreton, J. C.; Ramsahye, N. A.; Cohen, S. M.; Maurin, G. Understanding the Origins of Metal–organic Framework/Polymer Compatibility. Chem. Sci. **2018**, *9*, 315–324.

56. Mahajan, R.; Burns, R.; Schaeffer, M.; Koros, W. J. Challenges in Forming Successful Mixed Matrix Membranes with Rigid Polymeric Materials. J. Appl. Polym. Sci. **2002**, *86*, 881–890.

57. Li, Y.; Chung, T. S.; Cao, C.; Kulprathipanja, S. The Effects of Polymer Chain Rigidification, Zeolite Pore Size and Pore Blockage on Polyethersulfone (PES)-zeolite A Mixed Matrix Membranes. J. Membr. Sci. **2005**, *260*, 45–55.

58. Dong, G., Li, H.; Chen, V. Challenges and Opportunities for Mixed-matrix Membranes for Gas Separation. J. Mater. Chem. A **2013**, *1*, 4610-4630.

59. Loiseau, T.; Serre, C.; Huguenard, C.; Fink, G.; Taulelle, F.; Henry, M.; Bataille, T.; Férey, G. A Rationale for the Large Breathing of the Porous Aluminum Terephthalate (MIL-53) upon Hydration. Chem. Eur. J. **2004**, *10*, 1373–1382.

60. Rodenas, T.; van Dalen, M.; Serra-Crespo, P.; Kapteijn, F.; Gascon, J. Mixed Matrix Membranes Based on NH_2-functionalized MIL-type MOFs: Influence of Structural and Operational Parameters on the CO_2/CH_4 Separation Performance. Micropor. Mesopor. Mater. **2014**, *192*, 35–42.

61. Feijani, E. A.; Mahdavi, H.; Tavasoli, A. Poly(vinylidene fluoride) Based Mixed Matrix Membranes Comprising Metal Organic Frameworks for Gas Separation Applications. Chem. Eng. Res. Des. **2015**, *96*, 87–102.

62. Chen, X. Y.; Hoang, V. -T.; Rodrigue, D.; Kaliaguine, S. Optimization of Continuous Phase in Amino-functionalized Metal–organic Framework (MIL-53) Based Co-polyimide Mixed Matrix Membranes for CO_2/CH_4 Separation. RSC Adv. **2013**, *3*, 24266–24279.

63. Zornoza, B.; Martinez-Joaristi, A.; Serra-Crespo, O.; Tellez, C.; Coronas, J.; Gascon, J.; Kapteijn, F. Functionalized Flexible MOFs as Fillers in Mixed Matrix Membranes for Highly Selective Separation of CO_2 from CH_4 at Elevated Pressures. Chem. Commun. **2011**, *47*, 9522–9524.

64. Zhang, Y.; Feng, X.; Yuan, S.; Zhou, J.; Wang, B. Challenges and Recent Advances in MOF–polymer Composite Membranes for Gas Separation. Inorg. Chem. Front. **2016**, *3*, 896–909.

65. Wu, G.; Jiang, M.; Zhang, T.; Jia, Z. Tunable Pervaporation Performance of Modified MIL-53(Al)-NH_2/poly(vinyl alcohol) Mixed Matrix Membranes. J. Membr. Sci. **2016**, *507*, 72–80.

66. Bachman, J. E.; Smith, Z. P.; Li, T.; Xu, T.; Long, J. R. Enhanced Ethylene Separation and Plasticization Resistance in Polymer Membranes Incorporating Metal–organic Framework Nanocrystals. Nature Mater. **2016**, *15*, 845–849.

67. Sánchez-Laínez, J.; Zornoza, B.; Friebe, S.; Caro, J.; Cao, S.; Sabetghadam, A.; Seoane, B.; Gascon, J.; Kapteijn, F.; Guillouzer, C. L.; Clet, G.; Daturi, M.; Téllez, C.; Coronas, J. Influence of ZIF-8 Particle Size in the Performance of Polybenzimidazole Mixed Matrix Membranes for Pre-combustion CO_2 Capture and Its Validation Through Interlaboratory Test. J. Membr. Sci. **2016**, *515*, 45–53.

68. Abedini, R.; Omidkhah, M.; Dorosti, F. Highly Permeable Poly(4-methyl-1-pentyne)/NH_2-MIL 53 (Al) Mixed Matrix Membrane for CO_2/CH_4 Separation. RSC Adv. **2014**, *4*, 36522–36537.

69. Smith, Z. P.; Bachman, H. E.; Li, T.; Gludovatz, B.; Kusuma, V. A.; Xu, T.; Hopkinson, D. P.; Ritchie, R. O.; Long, J. R. Increasing M_2(dobdc) Loading in Selective Mixed-Matrix Membranes: A Rubber Toughening Approach. Chem. Mater. **2018**, *30*, 1484−1495.

70. C. Ordoñez, M. A.; Balkus Jr. K. J.; Ferraris, J. P.; Musselman, I. H. Molecular sieving Realized with ZIF-8/Matrimid® Mixed-matrix Membranes. J. Membr. Sci. **2010**, *361*, 28−37.

TOC

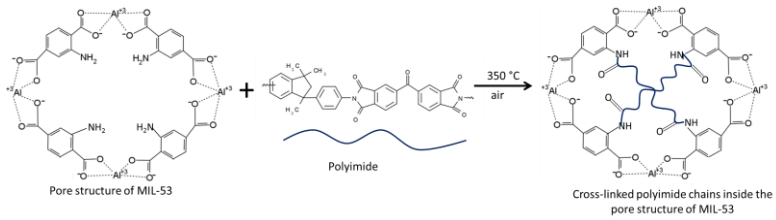
350 °C
air
Polyimide
Pore structure of MIL-53
Cross-linked polyimide chains inside the pore structure of MIL-53